Electronic Supplementary Material (ESI) for Physical Chemistry Chemical Physics.
This journal is © the Owner Societies 2017

# SUPPLEMENTARY INFORMATION

# FOR

# PHOTO-SWITCHING OF NON-IONIC AZOBENZENE AMPHIPHILE IN LANGMUIR AND LANGMUIR-BLODGETT FILMS

Emilia Piosik[a], Michał Kotkowiak[a], Izabela Korbecka[b], Zbigniew Galewski[b],
Tomasz Martyński[a1]

[a] *Faculty of Technical Physics, Poznan University of Technology, Piotrowo 3, 60-965 Poznań, Poland*
[b] *Faculty of Chemistry, University of Wroclaw, Joliot Curie 14, 50-383 Wrocław, Poland*

## DIFFERENTIAL SCANNING CALORIMETRY

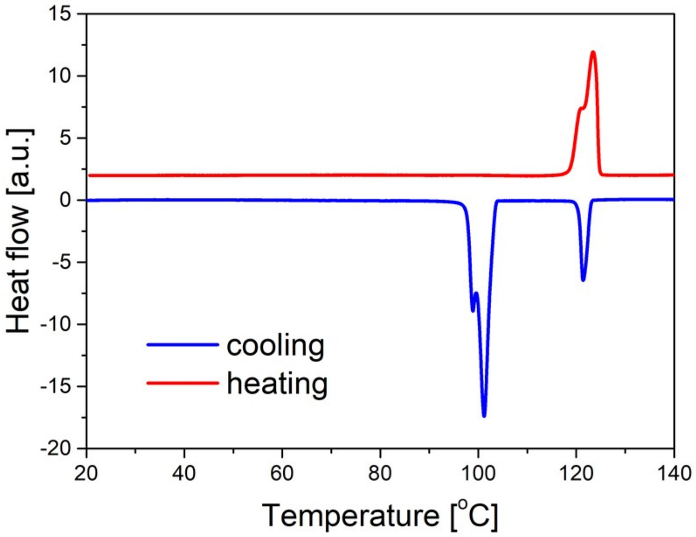

**Fig. S1.** DSC plots of LCA in heating (red line) and cooling modes (blue line).

---

[1] Corresponding author: tomasz.martynski@put.poznan.pl, Tel/Fax: +48 616653164

## EVALUATION METHOD OF PHOTOISOMERIZATION AND THERMAL RELAXATION RATE CONSTANTS

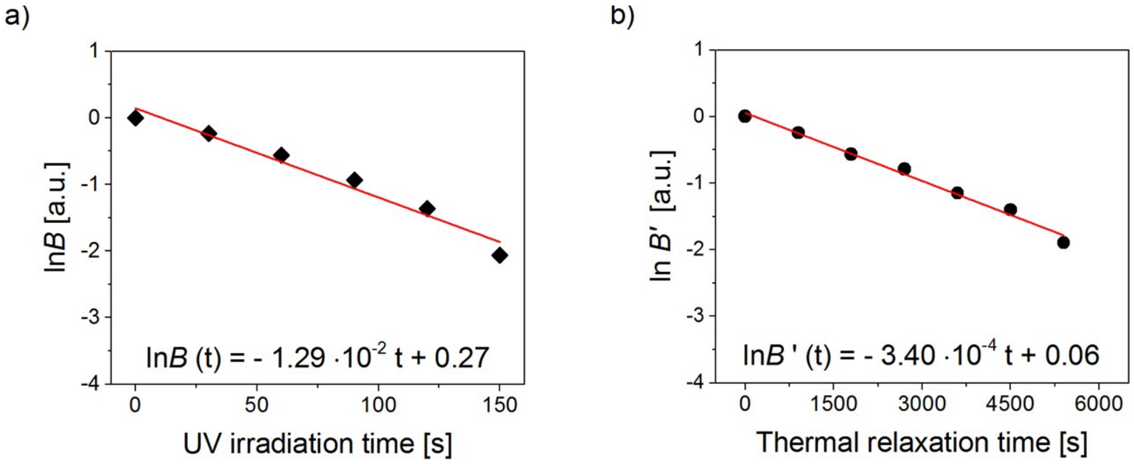

**Fig. S2.** Graphical illustration of the applied evaluation method of the photoisomerization (a) and thermal relaxation (b) rate constants.

## DENSITY FUNCTIONAL THEORY STUDIES

To improve the interpretation of the experimental results, the quantum mechanical calculations were done employing the Gaussian 09[1]. In all the calculations, the B3LYP hybrid functional (Becke 3-parameter exchange functional combined with Lee-Yang-Parr correlation functional) and the 6-31G(d) basis set for all atoms were used. The choice of the basis set was based on previous works for the azobenzene and its derivatives[2-5]. *Trans* and *cis* geometries were obtained by requesting a geometry optimization to a minimum. The initial *cis* geometries (for optimization to a minimum) were generated from optimized *trans* forms by changing the C-N=N-C dihedral angle. Relaxed scanning of the C-N=N-C dihedral angle of optimized *trans* structures allows to find corresponding stereoisomeric forms as well[2,3,6]. Transition-state structure was identified and confirmed by vibrational frequency analysis and a multistep process discussed in detail previously[6,7]. The time-dependent density functional theory (TD-DFT) calculations were performed using the equilibrium geometries of the molecules obtained from relaxed scanning to obtain UV-vis spectra. The influence of solvents, in particular chloroform, was taken into account using the Self-Consistent Reaction Field under Polarized Continuum Model (PCM). To convolute the resulting vertical excitation energies and oscillator strengths into the UV-Vis absorption spectra, the GaussSum program was used[8]. The spectra were generated assuming full width at half maximum of 3000 cm$^{-1}$ for all transitions. For clarity, the potential energy curve was calculated (Fig. S3) for isomerization of LCA in the chloroform by changing the dihedral angle from 0 to 180 degrees in 5 increments. The total energy and C-N=N-C dihedral angle were -3197143 kJ·mol$^{-1}$ and 0.5 deg., -3197082 kJ·mol$^{-1}$ and 174.5 deg. for *trans* and *cis* isomers, respectively.

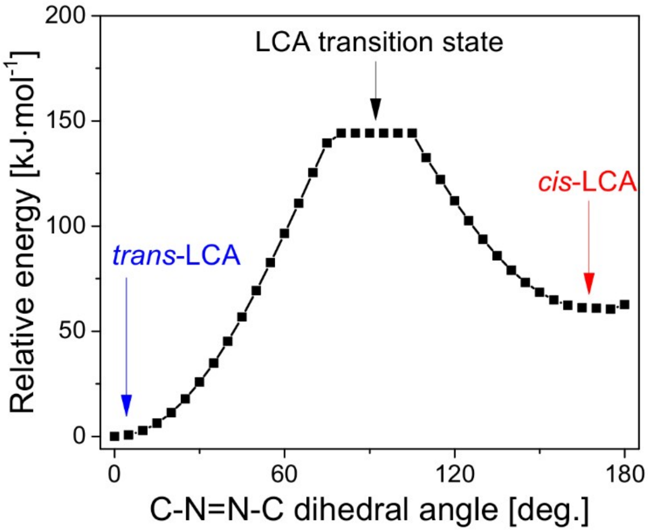

**Fig. S3.** Computed potential energy curve for thermal isomerisation of LCA along the C-N=N-C dihedral angle.

To obtain additional information on the electronic energy levels of LCA, the quantum-mechanical calculations were performed for the molecules in the *trans* and *cis* form. The position, oscillator strength and major contributions of the HOMO and LUMO levels are presented for both isomers in Table S1. Simulated electronic absorption spectra for the isomers in chloroform are presented in Fig. S4a. The spectra are with good agreement to the experimental ones (see Fig. 2 (a, c)) and have the same shape and character as these presented previously for azobenzene derivatives[9, 10]. However, it can be seen that experimental spectra are blue shifted in comparison to those simulated (44~nm and 26~nm, for *trans* and *cis* isomers, respectively). The differences between the experimental and computed spectra arise from the basis set used for the simulation which does not reflect all intermolecular interactions between the molecule and surrounding environment. The intense band in the UV range with the maximum at 388 nm for the *trans* isomer related to the $\pi$-$\pi^*$ transition (Fig. S4a) has oscillator strength (f) equal to 1.25, whereas the band in the visible range of the spectrum for the *cis* isomer with the maximum at 488 nm (the n-$\pi^*$ transition) has f=0.11. Furthermore, the $\pi$-$\pi^*$ and n-$\pi^*$ transitions are HOMO→LUMO transitions with a contribution equal to 100 and 85%, respectively. Moreover, the intense peak in the UV range for the *cis* isomer (339 nm) occurs due to the transition from HOMO-1 to LUMO with 72% contribution. HOMO-LUMO energy gap for *trans*-LCA is 3.50 eV and for *cis*-LCA 3.56 eV. Frontier molecular orbitals of investigated LCA in chloroform are shown in Fig. S5. The previous work by Pang *et al.*[10] for o-R-substituted (R=H, $CH_3$ $OCH_3$ or OH) 4,4'-diacetamidoazobenzene showed that for the double substituted *trans* molecule the redshift of the $\pi$-$\pi^*$ peak was observed in comparison to the unsubstituted system. Furthermore, they presented the azobenzene based photoswitching to be excited with green light for tetra substituted molecules. Moreover, for the tetra substituted *trans* nonpolar molecules the first vertical excitations were HOMO→LUMO transitions while both the vertical excitation for un- and tetra substituted *trans* forms were featured almost exclusively HOMO-1→LUMO transitions. The major contribution of the *cis* isomer did not depend on the subsitition[10] and were featured as HOMO→LUMO.

In order to understand the torsion effect of the azo unit on the spectral properties of LCA, we have performed the study on C-N=N-C dihedral angle on absorption spectra shown in Fig. S4b. Based on the potential energy curve shown in Fig. S3 and TD-DFT calculations we have plotted shorter and longer wavelength peak positions and values (Fig. S4b) *versus* the dihedral angle. The position of the shorter wavelength peak (closed black symbols) does not change gradually except for the transition isomer of LCA (dihedral angle from 80 to 105 deg.) and for the dihedral angle > 110 deg. blueshift is observed, whereas the peak value decreases with the dihedral angle except for the transition state. In the transition state only the shorter wavelength peak was observed in the UV-vis spectra. The longer wavelength peak position grows exponentially for the dihedral angle from 0 to 75 deg. and decreases in the same way for 110 to 180 deg. (closed red symbols). Furthermore, the peak value has the maxima for the longer wavelength peak at 30 deg. and 150 deg., respectively. Similar behavior of the azo unit on optical properties of the azobenzene derivatives was observed and reported previously. Ye *et al.*[9] have reported different changing tendency in the near UV and visible regions for three types of the azo derivatives. Similarly to our predictions, the absorption band in the visible region were more affected for the C-N=N-C dihedral angle (in a narrow range of angles). Furthermore, Liu *et al.*[11] showed that increasing π-conjugation extent lead to red shift of the corresponding absorption wavelength. Finally, it was confirmed by means of the TD-DFT calculation[9] that both dihedral angles could cause the increase of molecular dipole and π-conjugation extent, and thus led to the appearance of the absorption bands in the visible light region.

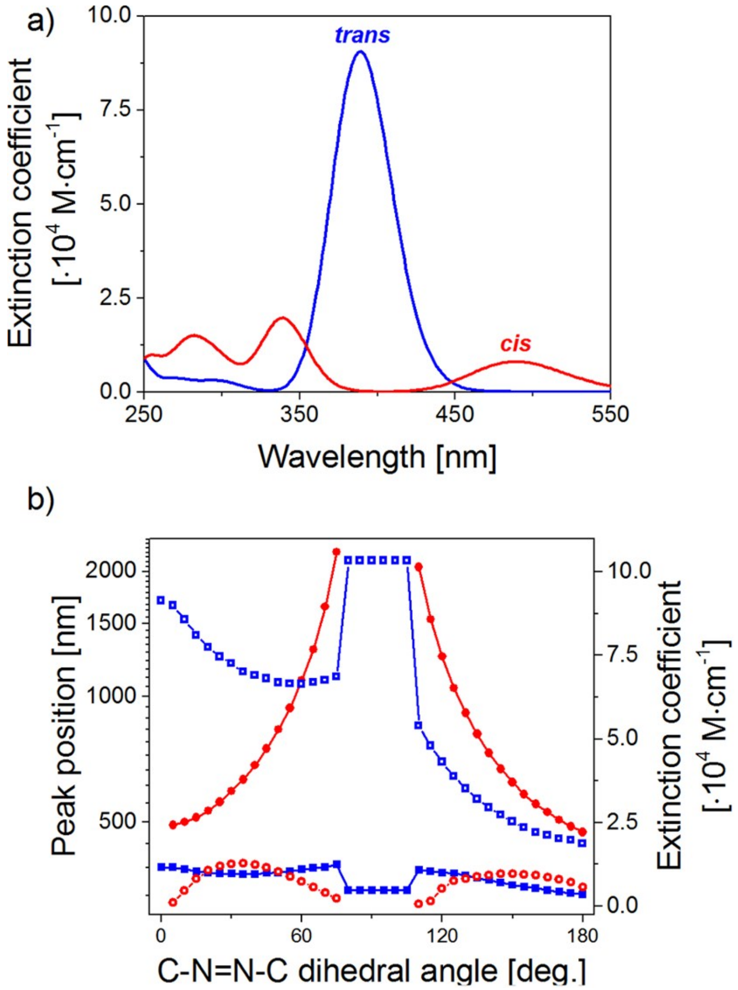

**Fig. S4.** Simulated absorption spectra of LCA in chloroform: (a) *trans* (blue line) and *cis* (red line) isomers, (b) the peak positions (closed symbols) and peak values (opened symbols) obtained from the absorption spectra *versus* the C-N=N-C dihedral angle for the shorter (black line) and longer (red line) wavelength peaks.

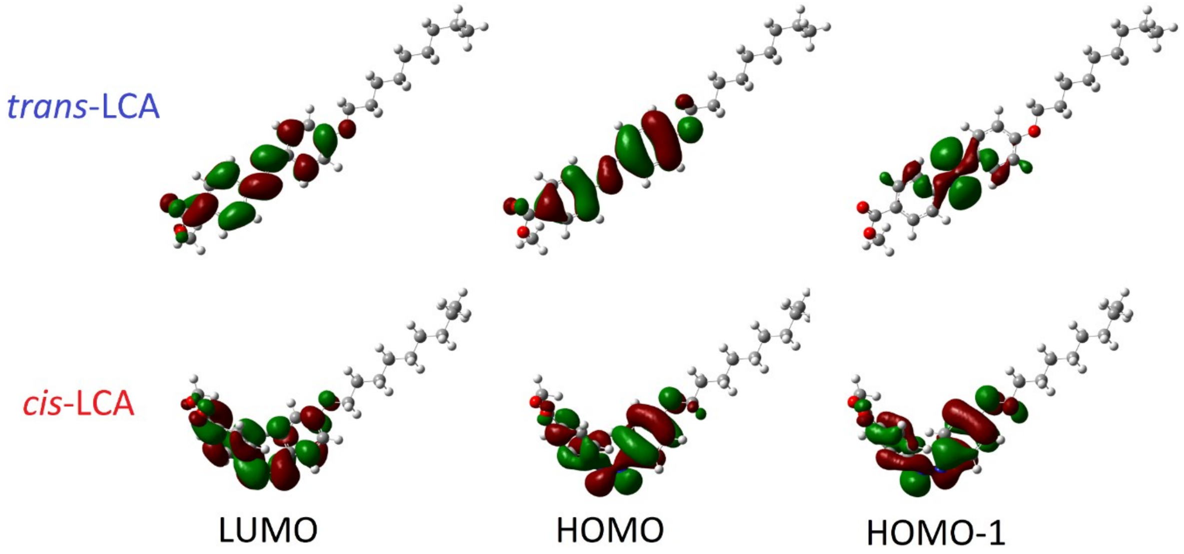

**Fig. S5.** Frontier molecular orbitals of LCA for *trans* and *cis* isomers obtained from TD-DFT calculations in chloroform.

**Table S1.** Selected electronic transitions calculated for LCA *trans* and *cis* isomers, respectively using the TD-DFT method. H – HOMO, L – LUMO.

| ***trans* isomer** | | |
|---|---|---|
| Wavelength [nm] | f | Major contribution |
| 484.7 | 0.0006 | H-1→L (98%) |
| 388.5 | 1.2506 | H→L (100%) |
| 305.6 | 0.01 | H-3→L (58%), H-2→L (34%) |
| 302.4 | 0.0147 | H-4→L (49%), H-3→L (21%), H-2→L (21%) |
| 290.5 | 0.0238 | H-5→L (10%), H-4→L (38%), H-3→L (11%), H-2→L (32%) |
| 271.1 | 0.0417 | H-5→L (67%), H→L+1 (18%) |
| 258.5 | 0.0018 | H-1→L+1 (95%) |
| 250.9 | 0.0514 | H-5→L (11%), H→L+1 (67%) |
| 244.2 | 0.0017 | H-1→L+2 (83%), H→L+2 (12%) |
| 242.9 | 0.0131 | H-6→L (34%), H-1→L+2 (15%), H→L+2 (42%) |
| 241.8 | 0.0054 | H-6→L (31%), H→L+3 (43%) |
| 240.5 | 0.1004 | H-6→L (27%), H-1→L+3 (10%), H→L+2 (25%), H→L+3 (25%) |
| 239.6 | 0.0151 | H-1→L+3 (88%) |
| 221.3 | 0.0075 | H-5→L+1 (26%), H-3→L+1 (22%), H-2→L+1 (29%) |
| 214.7 | 0.0184 | H-10→L (24%), H-4→L+1 (49%) |
| 212.8 | 0.0049 | H-10→L (52%), H-4→L+1 (13%) |
| 212.3 | 0.0001 | H-13→L (35%), H-12→L (20%), H-8→L (28%) |
| 211.3 | 0.0004 | H-13→L (13%), H-8→L (69%) |
| 208.3 | 0.0002 | H-9→L (94%) |
| 204.0 | 0.001 | H-18→L (28%), H-15→L (63%) |
| 203.1 | 0.0564 | H-3→L+1 (29%), H-2→L+1 (54%) |
| 200.8 | 0.0026 | H-1→L+4 (78%) |
| 200.4 | 0.003 | H-5→L+1 (32%), H-3→L+1 (28%) |
| 199.4 | 0.0024 | H-18→L (37%), H-15→L (15%), H-12→L (14%) |

***trans* isomer**

| Wavelength [nm] | f | Major contribution |
|---|---|---|
| 198.6 | 0.007 | H-3→L+3 (11%), H→L+4 (68%) |
| 198.4 | 0.0004 | H-18→L (12%), H-13→L (25%), H-12→L (52%) |
| 197.8 | 0.0447 | H-5→L+2 (18%), H-4→L+1 (16%), H-2→L+2 (35%) |
| 195.2 | 0.0016 | H-3→L+2 (25%), H-2→L+2 (12%), H-2→L+3 (30%) |

***cis* isomer**

| Wavelength [nm] | f | Major contribution |
|---|---|---|
| 488.4 | 0.1116 | H→L (85%) |
| 338.9 | 0.2696 | H-1→L (72%), H→L (13%) |
| 304.9 | 0.0502 | H-2→L (84%) |
| 295.5 | 0.0347 | H-3→L (74%), H→L+2 (16%) |
| 289.0 | 0.0766 | H-4→L (20%), H→L+1 (57%) |
| 278.8 | 0.084 | H-4→L (56%), H→L+1 (12%), H→L+2 (11%) |
| 272.5 | 0.0646 | H-3→L (11%), H→L+2 (66%) |
| 264.1 | 0.0221 | H-5→L (70%) |
| 254.2 | 0.0211 | H-4→L (10%), H→L+3 (80%) |
| 251.8 | 0.0962 | H-1→L+1 (89%) |
| 234.6 | 0.0245 | H-1→L+2 (74%) |
| 232.7 | 0.0128 | H-6→L (61%), H-3→L+1 (10%), H-2→L+1 (10%) |
| 229.2 | 0.0264 | H-6→L (33%), H-3→L+1 (32%), H-2→L+1 (12%) |
| 226.0 | 0.063 | H-4→L+1 (19%), H-2→L+1 (27%), H-2→L+2 (13%), H-1→L+2 (11%) |
| 222.6 | 0.0504 | H-1→L+3 (29%), H→L+4 (36%) |
| 221.3 | 0.0489 | H-1→L+3 (29%), H→L+4 (45%) |
| 216.7 | 0.0717 | H-10→L (13%), H-5→L+1 (24%), H-2→L+1 (15%), H-1→L+3 (21%) |
| 214.4 | 0.006 | H-10→L (59%) |
| 210.2 | 0.0033 | H-5→L+1 (38%), H-4→L+1 (14%), H-3→L+1 (17%), H-3→L+2 (12%) |
| 205.5 | 0.1721 | H-4→L+1 (19%), H-2→L+2 (65%) |
| 204.0 | 0.0067 | H-8→L (83%) |
| 203.1 | 0.0779 | H-13→L (16%), H-3→L+2 (37%) |
| 202.5 | 0.018 | H-13→L (26%), H-12→L (10%), H-3→L+2 (20%) |
| 200.9 | 0.0003 | H-9→L (91%) |
| 199.1 | 0.0385 | H-5→L+2 (20%), H-3→L+3 (13%), H-2→L+3 (49%) |
| 197.7 | 0.0003 | H-11→L (93%) |
| 197.5 | 0.0031 | H-4→L+2 (27%), H→L+5 (49%) |
| 196.1 | 0.0587 | H-4→L+2 (13%), H-3→L+3 (26%), H→L+5 (29%) |
| 195.5 | 0.0042 | H-15→L (44%), H-6→L+1 (27%) |

# *IN SITU* ABSORPTION MEASUREMENT

In Fig. S6, the absorption spectra of LCA recorded during compression of the *trans* (a) and *cis* (b) Langmuir films are presented in the function of the surface pressure. The course of the absorbance curve confim that the molecules of LCA remain in the proper isomeric form during the whole compression process.

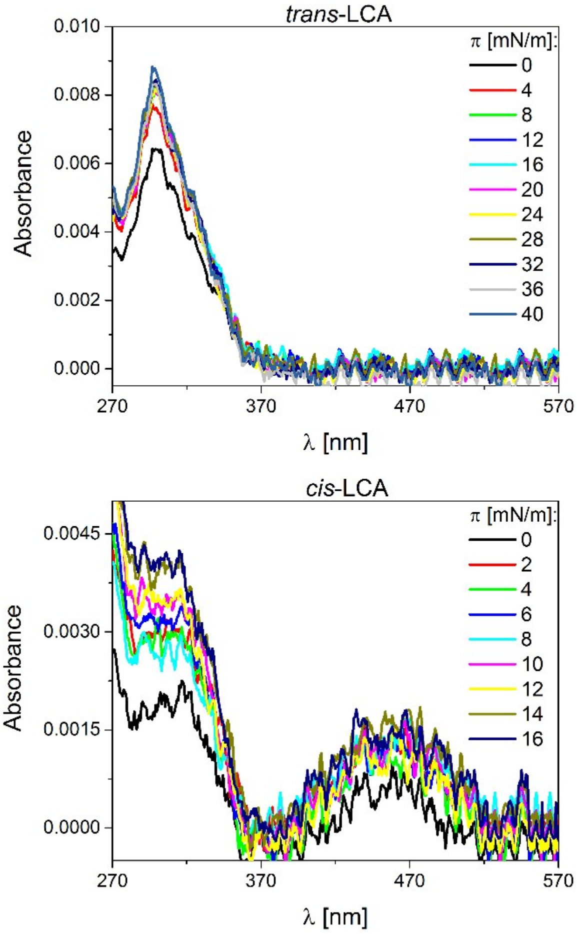

**Fig. S6.** Absorption spectra recorded *in situ* during compression of the Langmuir monolayers formed by LCA in *trans* (a) and *cis* (b) isomeric form at the different surface pressure values.

# ATOMIC FORCE MICROSCOPY

The AFM height images of the LCA LB film deposited onto the glass substrate in *cis* form and thermally relaxed to the *trans* form were recorded before and after its UV light irradiation for 5 min in order to show the change of the sample morphology in nanoscale as a result of the photoisomerization process. They are presented in Fig. S7a and Fig. S7b, respectively, together with their cross-section profiles. However, we did not observe significant change in the LCA film morphology or in the size of the visible grains. The average height of the domains is equaled to (3.3±0.8) nm before and (3.4±0.8) nm after the UV irradiation irradiation. Also the average roughness (RMS) is very similar in both cases and takes the value of 0.91. The reason of these observations is a fact that during scanning of organic LB films a cantilever tip of the AFM in the tapping mode touches soft part of molecules – usually alkyl chains-causing their bending.

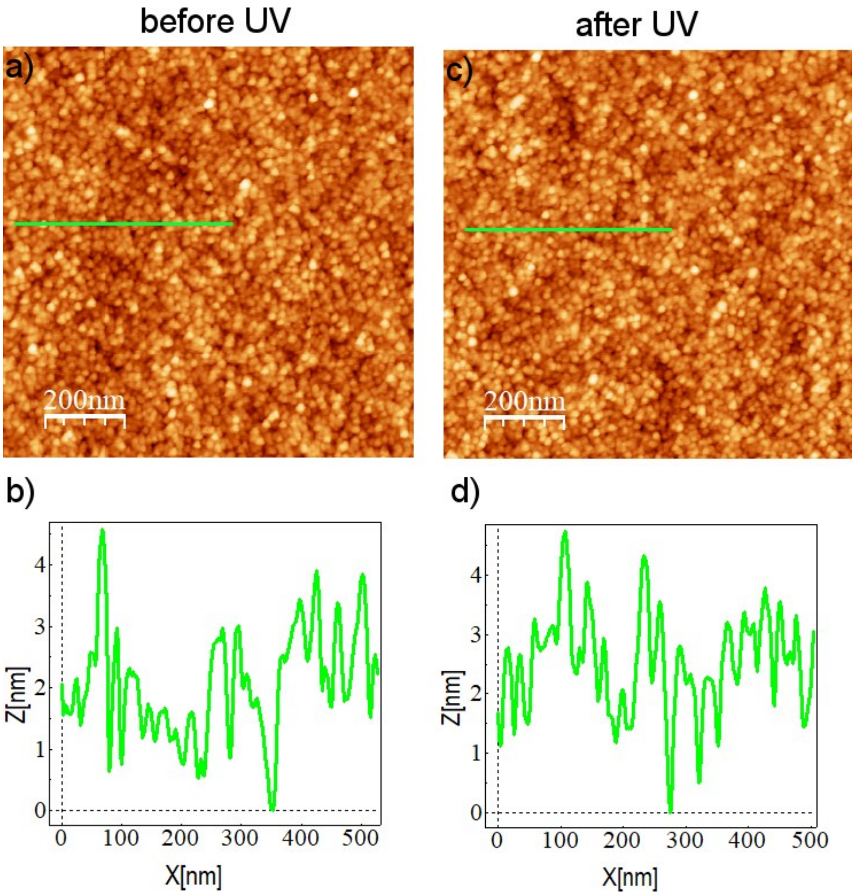

**Fig. S7.** AFM images with corresponding cross-section profiles of the LCA LB film deposited onto the glass substrate in the *cis* form at the surface pressure of 10 mN·m$^{-1}$ and thermally relaxed to *trans* form recorded before (a, b) and after its UV light irradiation for 5 min (c, d).

# REFERENCES

1 M. J. Frisch, G. W. Trucks, H. B. Schlegel, G. E. Scuseria, M. A. Robb, J. R. Cheeseman, G. Scalmani, V. Barone, B. Mennucci, G. A. Petersson, H. Nakatsuji, M. Caricato, X. Li, H. P. Hratchian, A. F. Izmaylov, J. Bloino, G. Zheng, J. L. Sonnenberg, M. Had and D. J. Fox, *Gaussian 09, Revision E.01*, Gaussian, Inc., Wallingford CT, 2009.

2 J. Fu and M. Barra, *Trends Org. Chem.*, 2012, **16**, 1–8.

3 R. Tabone and M. Barra, *Dyes Pigm.*, 2011, **88**, 180–186.

4 M. Dubecký, R. Derian, L. Mitas and I. Štich, *J. Chem. Phys.*, 2010, **133**, 24–28.

5 J. Dokić, M. Gothe, J.Wirth, M. V. Peters, J. Schwarz, S. Hecht and P. Saalfrank, *J. Phys. Chem. A*, 2009, **113**, 6763–6773.

6 S. K. Rastogi, R. A. Rogers, J. Shi, C. Gao, P. L. Rinaldi and W. J. Brittain, *J. Org.Chem.*, 2015, **80**, 11485–11490.

7 N. A. Wazzan, P. A. Richardson and A. C. Jones, *Photochem. Photobiol. Sci.*, 2010, **9**, 968–974.

8 Steffen, K. Thomas, U. Huniar, A. Hellweg, O. Rubner and A. Schroer, *J.Comput. Chem.*, 2010, **31**, 2967–2970.

9 Y. Ye, J. Pang, X. Zhou and J. Huang, *Comp. Theor. Chem.*, 2016, **1076**, 17–22.

10 J. Pang, Z. Tian and J. Ma, *Chem. Phys. Lett.*, 2014, **613**, 110–114.

11 R. Liu, Y. Li, J. Chang, Q. Xiao, H. Zhu and W. Sun, *J. Photochem. Photobiol. A*, 2012, **239**, 47–54.